Journal of Applied Polymer Science

Ultrafine fly ash as a reinforcing filler in poly(lactic acid) matrix

Bai Xue, Jianjun Bao, Junhua Zhang
State Key Laboratory of Polymer Materials Engineering, Polymer Research Institute, Sichuan University, Chengdu 610065, China
Correspondence to: J. Zhang (E-mail: zhangjh@scu.edu.cn)

ABSTRACT: Fly ash, inexpensive and not eco-friendly material, is the residue from the coal burning in thermal power stations. If ways can be found to use it, it will facilitate applications for the ash materials and simultaneously reduce the pollution. In this study, silane-grafted ultrafine fly ash (S-UFA) was used as a reinforcing filler in poly(lactic acid) (PLA) to prepare a series of PLA/S-UFA composites. The tensile strength of PLA/S-UFA composites increases with the increase of S-UFA content when less than 20 wt %; after a loading fraction greater than 30 wt %, the tensile strength of the composites decreases with the increasing S-UFA weight fraction. The morphology of PLA/S-UFA composites was observed by scanning electron microscope (SEM). X-ray diffraction (XRD) analysis was applied to investigate the crystal structure of S-UFA and the composites. The thermal properties of these composites were studied by thermogravimetric analysis (TGA) and differential scanning calorimetry (DSC). The TGA results showed that the thermal stability of PLA/S-UFA composites slightly decreased with the increasing S-UFA loading fraction. © 2016 Wiley Periodicals, Inc. J. Appl. Polym. Sci. **2016**, *133*, 43716.

KEYWORDS: blends; grafting; mechanical properties

Received 18 January 2016; accepted 31 March 2016
DOI: 10.1002/app.43716

INTRODUCTION

Poly(lactic acid) (PLA) is one of the most extensively investigated and utilized bio-based polymers due to its ideal attractive properties such as thermoplasticity, processability, renewability, biocompatibility, good mechanical properties, and low environmental impact.[1–4] PLA, a kind of linear aliphatic thermoplastic polyester derived from renewable resources, is considered as a solution to relieve the dependence on traditional petroleum-based plastics. It can be produced either by catalytic ring opening polymerization of lactides (lactic acid dimers) or by condensation polymerization of lactic acid monomers which are obtained from the fermentation of sugar feed stocks.[5–7] Lactic acid exists as two enantiomeric forms, the naturally occurring L (−) configuration and the D (+) configuration. Therefore, the corresponding enantiomeric polymers are produced by the conservation of the chiral centers.[8] PLA with high strength and high modulus can be easily processed by a number of processing methods (e.g., foaming, extrusion, injection molding, blow molding, fiber spinning, film forming, and compression molding)[9–11] to yield articles to be used in biocompatible/bioabsorbable market, for example, surgical implants, sutures drug delivery systems, and dentistry.[12,13] Moreover, lots of efforts have been currently made to use PLA as engineering material, for example, automobile components, building materials, and electric appliance bodies.[11,14] However, the high price, inherent brittleness and thermal instability of PLA currently limit its application.[15–17] Considerable efforts have been made to improve these shortcomings of PLA.[18–21]

Fly ash, a gray powder with different size fractions, is the residue generated from coal fired thermal power stations. Larger numbers of coal fired power plants in the world produce a huge quantity of fly ash, creating a terrible environmental problem that needs to be addressed. Less than half of the ash is applied as a raw material of concrete; the remaining is directly disposed in the landfill or simply piled up.[22] New ways of utilizing fly ash have attracted a considerable research interest. The utilization of fly ash is influenced by their properties, for example, fineness, hardness, particle shape, particle size, specific surface area, etc. A particularly advantageous and promising utilization of fly ash is as a filler into polymer matrix, where an average size fraction of 5 μm was verified to be suitable for this purpose.[23] Ultrafine fly ash (UFA) with a particle size of 5 μm is obtained from advanced grading techniques such as a series of cyclones. It has been found that the mechanical properties of plastic products containing UFA are improved. UFA can supplement the bulk volume of the polymer itself and facilitate processing of custom-shaped products. It is important for UFA to combine properly with the polymeric matrix to which it is introduced, and be nontoxic to any polymerization reaction taking place in the polymer during the processing.

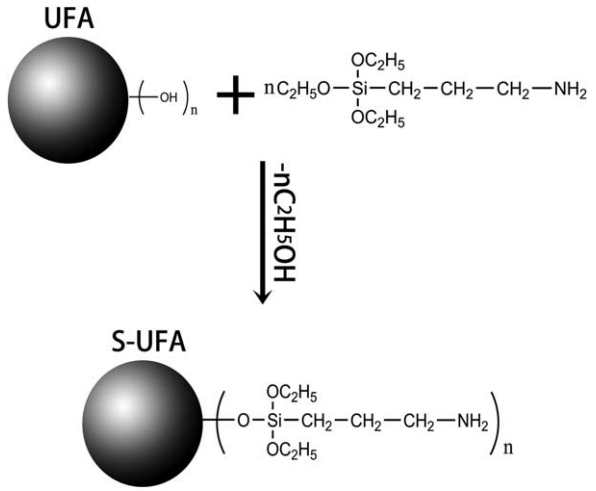

Figure 1. The mechanism of synthesis of S-UFA.

Fly ash is mainly applied as a raw material for concrete manufacturing and construction. To the best of our knowledge, the introduction of UFA into biodegradable polymer matrix as a reinforcing filler is rarely reported. In this article, silane-grafted UFA (S-UFA) as a reinforcing filler was introduced into PLA matrix to prepare a series of PLA/S-UFA composites. It can facilitate applications for UFA and simultaneously reduce the environmental pollution. Scanning electron microscope (SEM) was applied to study the morphology of PLA/S-UFA composites. The crystal structure of PLA/S-UFA was characterized by X-ray diffraction (XRD). The mechanical and thermal properties of the composites were investigated by tensile test, differential scanning calorimetry (DSC), and thermogravimetric analysis (TGA).

EXPERIMENTAL

Materials

Poly(lactic acid) (PLA), which consists of about 2% D-lactide units, was obtained from Nature Works LLC (The United State). PLA presents molecular mass $M_w = 197$ kDa and a density of 1.24 g/cm^3. Ultrafine fly ash (UFA) with the particle size of around 5 μm was purchased from Guizhou Mingchuan Fly Ash Co., Ltd (China). About 50% of the UFA particles remain fine sphere shape. 3-Amino propyl triethoxy silane (APTES) was purchased from Chengdu Kelong Chemical Reagent Co., Ltd (China).

Silane Grafting

Silane-grafted UFA (S-UFA) was prepared by grafting APTES onto the surface of UFA. The mechanism of synthesis of S-UFA is shown in Figure 1. A certain quantity of UFA was introduced into the mixture of water/ethanol (20:80 wt %) with a magnetic agitation and the temperature was hold at 80 °C. Subsequently, 2 wt % APTES based on UFA was added into the aforementioned mixture and continuously agitated at 80 °C for 5 h. The resultant products were filtered and washed with large amounts of water. At last, the products were dried at 80 °C overnight.

Sample Preparation

Prior to blending, PLA pellets were dried at 85 °C for 12 h in the oven to remove moisture in the raw materials. The PLA and S-UFA were premixed by simple mechanical blending. The composites were prepared by Brabebder (Duisburg, Germany) internal mixer at 180 °C for 8 min and at a screw speed of 40 rpm. Then, the specimens used for measurements were compression-molded under the pressure of 10 MPa and at 185 °C for 8 min, and then cooled instantly to room temperature under the same pressure. Therefore, a series of PLA/S-UFA composites containing 0, 10, 20, 30, 40, and 50 wt % were prepared. For the sake of comparison, a series of PLA/non-silane grafted UFA (PLA/UFA) composites were obtained under the same processing conditions as described above.

Measurements

Fourier Transform Infrared Spectroscopy. The FTIR spectra of UFA and S-UFA were obtained from a Thermo Electron Corporation Nicolet 6700 FTIR spectrometer (The United States). A total accumulation of 24 scans and a resolution of 4 cm^{-1} were adequate to obtain high signal-to-noise spectra in the range of 4000–500 cm^{-1}.

Mechanical Properties. Tensile characterization was carried out on a tensile tester (INSTRON-5567, The United States) according to ASTM D 638-08. The crosshead speed was 5 mm/min. The samples with a dumbbell type were placed at ambient temperature and atmospheric condition for 2 days before test. Five tests were taken for the average value.

A ZBC-4B izod impact tester (Shenzhen Xinsi Co., Ltd, China) was applied to investigate the notched izod impact characterizations of the composites according to ASTM D 256-06. The size of samples for the measurement was 80 × 10 × 4 mm^3. There was a depth of 2 ± 0.2 mm notch in the middle of each sample. An average value of five tests was taken for each sample.

Morphology of PLA/UFA Composites. The morphology of UFA and PLA/S-UFA blends was observed by a scanning electron microscope instrument (JSM-5900, JEOL, Japan). The samples were cooled in liquid nitrogen and then fractured. For SEM texting, all the fractured surfaces were coated with a thin layer of gold to prevent electrostatic charging.

X-ray Diffraction Analysis. To study the crystalline structure of the blends, XRD scans of the S-UFA, pure PLA and PLA/S-UFA composites were performed on a D/MAX-III X-ray diffractometer at a generator voltage of 50 kV. The scattering angle range was $2\theta = 5°$–$60°$ and the scanning speed was 0.06°/s.

Differential Scanning Calorimetry. The melting and crystallization characterizations of the blends were studied using a differential scanning calorimeter (DSC-204, Netzsch, Germany) under a nitrogen flow of 40 mL/min. The temperature of the DSC apparatus and the heat of fusion were calibrated with indium. Experiments were carried out with 7–8 mg samples in aluminum sample pans. Firstly, the samples were held at 30 °C for 5 min, and then scanned from 30 °C to 200 °C at a heat rate of 10 °C/min. Subsequently, the samples were held at 200 °C for 3 min, and then cooled at a rate of 5 °C/min to 30 °C. The crystallinity of the composites was calculated with eq. (1):

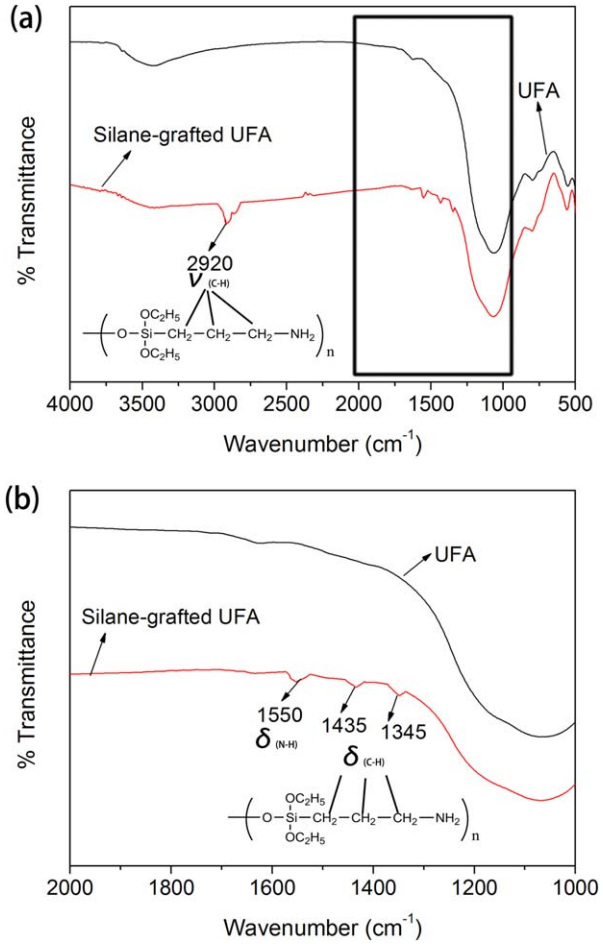

Figure 2. (a) FTIR spectra of UFA and S-UFA in the region of 4000–500 cm^{-1} and (b) the magnified versions in the region of 2000–1000 cm^{-1}. [Color figure can be viewed in the online issue, which is available at wileyonlinelibrary.com.]

$$X_c\ (\%) = \frac{\Delta H_m}{\Phi \Delta H_0} \times 100 \quad (1)$$

where, X_c is the degree of crystallinity, ΔH_0 with a value of 93.7 J/g is the theoretical melting enthalpy for 100% crystalline PLA.[8,24] ΔH_m stands for the crystal melting heat of samples. Φ denotes the weight fraction of PLA in the composites.

Thermogravimetric Analysis. Thermogravimetric analysis (TGA) was carried out on a TGA analyzer (TG 209F1, Germany) at a purge rate of 60 mL/min under the nitrogen atmosphere. The samples of 10–20 mg were heated from 30 °C to 600 °C at a rate of 10 °C/min. The relative mass loss of the materials was recorded as a function of temperature during the heating process.

RESULTS AND DISCUSSION

FTIR Spectroscopy

Figure 2(a) shows the FTIR spectra of UFA and S-UFA in the region of 4000–500 cm^{-1}. Figure 2(b) shows the magnified versions in the region of 2000–1000 cm^{-1}. The C—H stretching vibration of propyl groups is present at 2920 cm^{-1}. The band observed at 1550 cm^{-1} is attributed to —NH2 deformation mode.[25] The bands centered at 1435 and 1345 cm^{-1} correspond to the methylene deformation modes of propylamine.[26] The characteristic peaks of APTES are observed in the spectrum of S-UFA, which illustrates that APTES has been successfully grafted onto the surface of UFA.

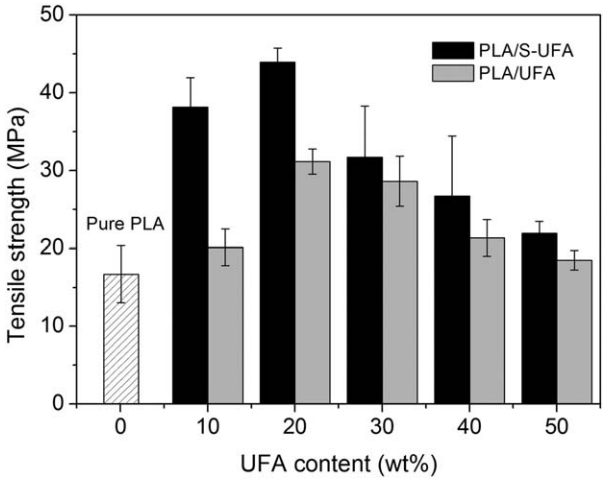

Figure 3. Tensile strength of PLA composites with different contents of ultrafine fly ash (UFA).

Mechanical Properties

The tensile strength of the composites was investigated, as shown in Figure 3. The tensile strength of both PLA/S-UFA and PLA/UFA composites increases with the increase of UFA content when less than 20 wt %; after a loading fraction greater than 30 wt %, the tensile strength of the composites decreases with the increasing UFA weight fraction. The maximum tensile strength of 43.9 MPa for PLA/S-UFA composites is achieved at the S-UFA loading fraction of 20 wt %, which is 1.6 times higher than that of pure PLA. However, the maximum tensile strength for PLA/UFA composites is only 31.16 MPa at the same UFA content. The effective reactive compatibilization between the amine groups on the S-UFA particles and the strong polar groups of PLA largely improves the interfacial adhesion between

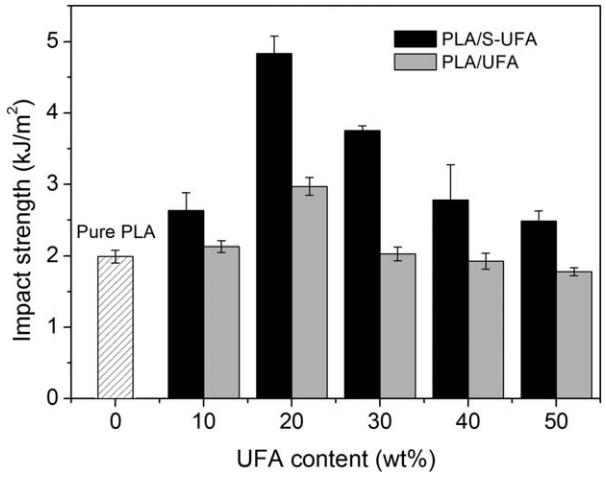

Figure 4. Impact strength of PLA composites as a function of UFA content.

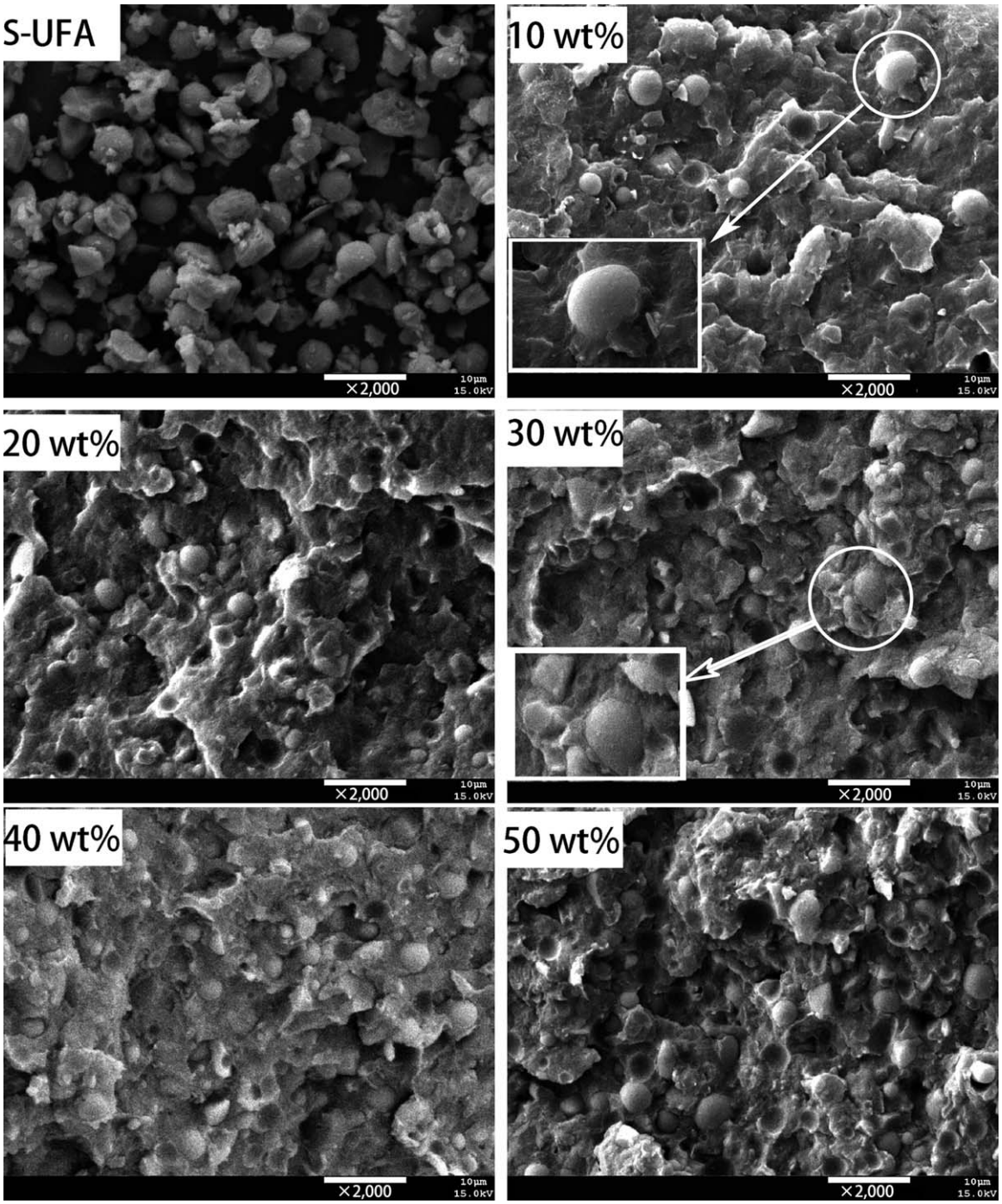

Figure 5. SEM images of S-UFA and cryo-fractured surfaces of the PLA/S-UFA composites.

S-UFA and PLA matrix, which leads to the considerable enhancement in the tensile strength of PLA/S-UFA composites. Thus, S-UFA can be as rigid particles to enhance the tensile strength of PLA. When UFA loading exceeds 30 wt %, the tensile strength decreases gradually, which is possibly attributed to the aggregation of UFA. Generally speaking, as the amount of filler increases, the aggregation will take place more easily. Then, the regions of stress concentration that come into being with the aggregation will propagate the cracks at a lower stress.[27] During the tensile testing, these flaws retard the effective transfer of the stress and finally lead to the fracture of the samples. However, in the UFA content region higher than 30 wt %, the tensile strength of PLA/S-UFA is also higher than that of PLA/UFA, which further confirms that silane grafting is an effective method to improve the interfacial adhesion between UFA particles and PLA matrix.

Figure 4 shows the effect of the loading fraction of UFA on the impact strength of the composites. The maximum impact strength of 4.83 kJ/m^2 for PLA/S-UFA composites is obtained at

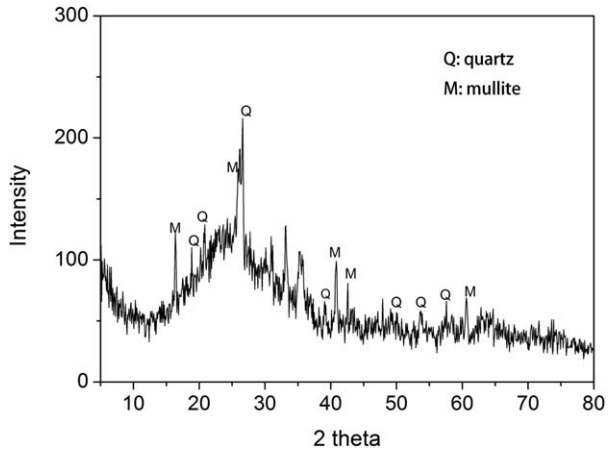

Figure 6. The XRD patterns of S-UFA.

the S-UFA loading fraction of 20 wt %, which is 1.43 times higher than that of pure PLA. However, the maximum impact strength for PLA/UFA composites is only 2.97 kJ/m^2. The superior impact property of PLA/S-UFA composites is attributed to the fact that silane treatment improves the filler surface adhesion characteristics by grafting large numbers of amine groups onto the surface of UFA. The increasing filler/matrix interfacial adhesion provides effective resistance to crack propagation and thereby improves the toughness of these composites. After the UFA loading fraction greater than 30 wt %, the impact strength of the composites decreases with the increase of UFA content. This demonstrates that the aggregation of UFA particles begins at 30 wt % content, or more specifically, between 20 and 30 wt %. The addition of high filler content increases the probability of filler agglomeration, which leads to the immiscible dispersion of UFA particles within PLA and a subsequent strong weakening effect. It is clearly seen that the tendency of the impact strength with the UFA loading fraction is similar to that of tensile strength.

Morphology of the PLA/S-UFA Composites

The SEM images of S-UFA and the cryo-fractured surfaces of PLA/S-UFA blends are shown in Figure 5. Representative figure S-UFA shows that S-UFA particles exhibit a size of around 5 μm and 30%–50% of them remain good spherical shape. These S-UFA particles have good dispersion without aggregation. As shown in the photographs of the cryo-fractured surfaces of the blends, it is illustrated that S-UFA particles are dispersed in PLA matrix well. And in the inlet photo of figure 10 wt %, it is clearly seen that the interfacial adhesion between S-UFA and PLA matrix is pretty good. Optimizing the interface between the UFA particles and PLA matrix through the use of silane coupling agents could enhance the mechanical properties of the composites.

X-ray Diffraction Analysis

The XRD characterization was carried out to determine crystal structures of S-UFA and PLA/S-UFA composites. SO_2 and Al_2O_3 are the major components of fly ash, corresponding to 55.2 and 25.4 wt %, respectively.[28] Fe_2O_3, CaO, MgO, MnO, and other oxides essentially contribute to the remaining portion. The XRD pattern for S-UFA is shown in Figure 6. It consists of two major phases of quartz (SiO_2) and mullite ($Al_6Si_2O_{13}$), consistent with the major components of fly ash. It is observed that the strongest characteristic peaks of the two phases of quartz and mullite appear at $2\theta = 26.68°$ and 26.01°, respectively.[28] This demonstrates that silane grafting has little influence on the crystal structures of UFA.

The results of the XRD analysis for pure PLA and PLA/S-UFA composites are shown in Figure 7. All the samples exhibit two typical diffraction peaks at about $2\theta = 16.5°$ and 18.9°, according to the (200)/(100) and (203) planes of the PLA α crystal.[29] It is clearly seen that the introduction of S-UFA into PLA matrix has little influence on the crystalline forms of PLA. As shown in the inlet figure, the characteristic diffraction peaks of the quartz and mullite phases are also observed in the PLA/S-UFA composites, which are attributed to the crystalline forms deriving from the introduced S-UFA. It illustrates that S-UFA could maintain original crystalline forms in the PLA/S-UFA blends.

Differential Scanning Calorimetry

Figure 8 shows the heating and cooling DSC curves of the neat PLA, PLA/S-UFA composites. For clarity, all of the DSC scan curves are shifted vertically. The observed melting temperature (T_m), crystallization temperature (T_c), melting enthalpy (ΔH_m), and crystallinity (X_c) for PLA are summarized in Table I.

From Figure 8(a), double endothermic peaks, low- and high-temperature peaks, are evidently observed in all the heating DSC curves of the samples. The origin of the double melting behavior could be explained by the melt–recrystallization model: The melting of PLA proceeds through the melting of original crystals, recrystallization, and the melting of recrystallized crystals.[30] As for pure PLA and its composites, the crystallinity is relatively low and less perfect crystals are formed, thus the samples go through the melting–recrystallization–remelting process upon heating. The low-temperature peak at about 164 °C originates from the melting of original crystals; the higher-temperature peak at the temperature of 168 °C is attributed to the melting of recrystallized crystals.[30] This phenomenon,

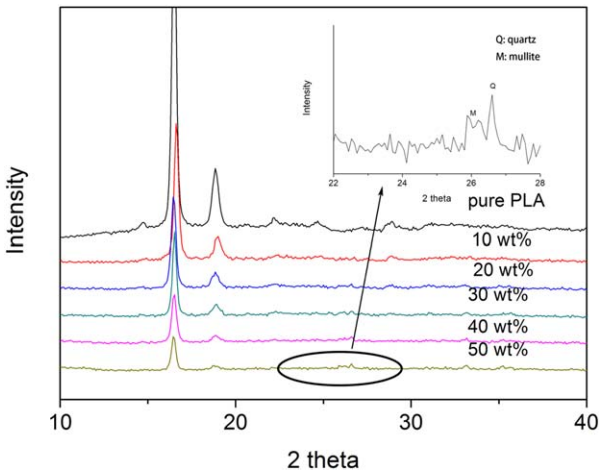

Figure 7. The XRD comparison patterns of pure PLA and PLA/S-UFA composites. [Color figure can be viewed in the online issue, which is available at wileyonlinelibrary.com.]

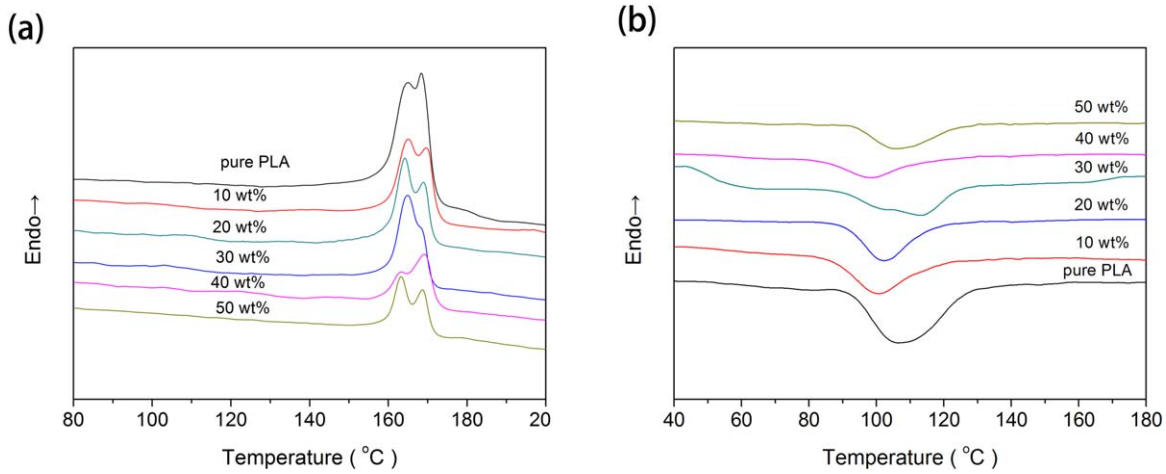

Figure 8. (a) DSC heating curves and (**b**) DSC cooling curves obtained from PLA/S-UFA composites. [Color figure can be viewed in the online issue, which is available at wileyonlinelibrary.com.]

Table I. The Melting Temperature, Crystallization Temperature, Melting Enthalpy, and Crystallinity of Pure PLA and PLA/S-UFA Composites

S-UFA content (wt %)	T_m (°C)	T_c (°C)	ΔH_m (J/g)	X_c (%)
0	164.5, 168.3	105.6	41.61	44.4
10	164.8, 169.3	101.4	22.63	26.8
20	164.7, 168.3	102.3	21.85	29.1
30	164.2, 168.8	102.4	19.41	29.5
40	163.4, 169.1	99.6	13.24	23.5
50	163.2, 168.5	103.7	9.02	19.25

similar double melting behaviors, has been reported in many semi-crystalline polymers. The crystallinity for PLA drastically decreases from 44.4% to 26.8% with the introduction of 10 wt % S-UFA. It is suggested that S-UFA particles lessen the mobility of PLA chains and subsequently retard the crystallization of the polymer. The crystallinity of the composites increases slightly with the increasing S-UFA loading fraction at 10–30 wt %. After a loading fraction greater than 30 wt %, the crystallinity declines sharply again, which is ascribed to the aggregation of the S-UFA particles.

Figure 8(b) shows that a single exothermic peak appears in each curve during the cooling process. The crystallization exothermal peak becomes much milder with the increase of S-UFA loading fraction, which also indicates that crystallinity capacity of the composites declines with the incremental S-UFA content. The crystallization temperature of pure PLA is about 105.6 °C and shifts to a little lower temperature with the introduction of S-UFA particles. It is easy to understand that S-UFA particles slow down the crystallization process by decreasing the mobility of PLA chains.

Thermogravimetric Analysis

The thermal stability and decomposition of neat PLA and PLA/S-UFA composites were investigated by thermogravimetric analysis (TGA) under nitrogen atmosphere. Figure 9 shows the residual weight and derived weight as a function of temperature for PLA/S-UFA composites. The representative TGA data of the

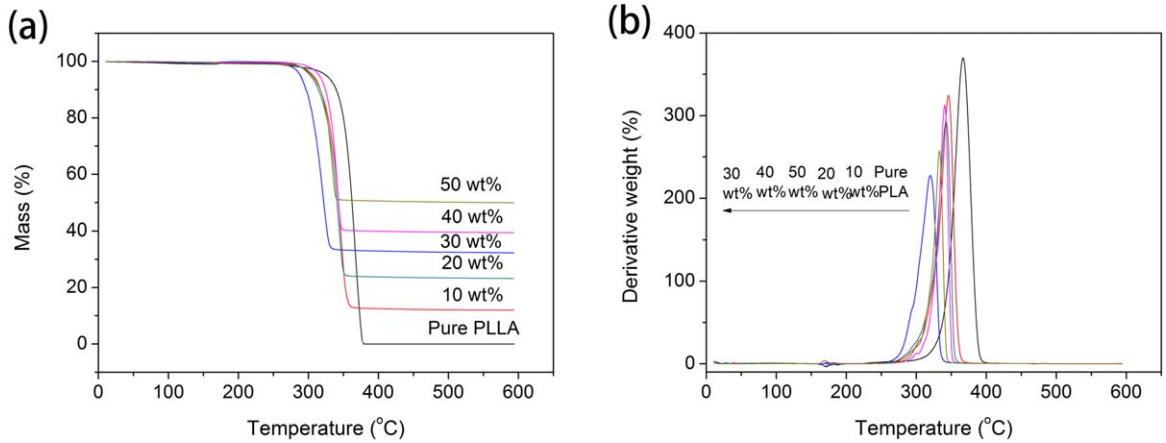

Figure 9. (a) TGA and (b) DTG thermograms of the pure PLA and PLA/S-UFA composites. [Color figure can be viewed in the online issue, which is available at wileyonlinelibrary.com.]

Table II. TGA T_{onset}, T_{max}, and R_e Values of the Neat PLA and PLA/S-UFA Composites

S-UFA content (wt %)	T_{onset} (°C)	T_{max} (°C)	R_e (%)
0	349,6	366.5	0.52
10	327.6	345.9	12.02
20	323.8	342.6	23.33
30	300.1	319.8	32.33
40	327.3	332.7	39.44
50	320.3	337.9	49.89

samples are listed in Table II. The maximum weight loss temperature (T_{max}) is taken from the peak value of the derivative thermogravimetry (DTG) thermograms, whereas the onset decomposition temperature (T_{onset}) is determined from these curves by extrapolation from the peak of degradation back to the initial weight of the polymer. The eventual residual weight percentage (R_e) is obtained from the TGA thermograms. All of the TGA data for PLA and PLA/S-UFA blends exhibit similar tendency. The T_{onset} slightly declines as S-UFA particles are introduced into PLA matrix, which indicates that the addition of S-UFA deteriorates the thermal stability of the blends. The most probable reason is that the metal oxide components of S-UFA catalyze the degradation of PLA. However, after the S-UFA loading fraction greater than 30 wt %, T_{onset} begins to increase with the increasing S-UFA content. This could be ascribed to the barrier effect of the S-UFA particles against the volatile pyrolyzed products. S-UFA particles have aggregated at the S-UFA loading weight fraction of 30 wt %, confirmed by the morphology of PLA/S-UFA blends. Furthermore, the barrier effect against the volatile pyrolyzed products is vastly enhanced with the aggregation of S-UFA particles. It is clearly seen that the T_{max} of the composites has the same regularity with the T_{onset}. The T_{max} of PLA is 366.5 °C and unexpectedly declines to 345.9, 342.6, 319.8, 332.7, and 337.9 °C, respectively, with the increasing S-UFA loading fraction.

CONCLUSIONS

In this article, a series of poly(lactic acid)/silane-grafted ultrafine fly ash (PLA/S-UFA) composites were prepared via melt blending process by S-UFA filling PLA. The tensile strength of PLA/S-UFA composites reaches the highest value of 43.9 MPa at the 20 wt % S-UFA content, and then decreases with the incremental S-UFA loading fraction. This is possibly due to the aggregation of S-UFA particles at 30 wt % S-UFA content, which is confirmed by the SEM images. Good dispersion of S-UFA particles into the matrix and pretty interfacial adhesion between them were confirmed by the morphological study carried on SEM. The crystal structures of S-UFA and the PLA/S-UFA composites were investigated by XRD analysis. DSC measurements deduce that the crystallinity of PLA decreases with the increase of S-UFA loading fraction. Because the introduced S-UFA particles reduce the mobility of PLA chains and subsequently retard the crystallization of PLA. TGA shows the addition of S-UFA slightly deteriorates the thermal stability of the composites, which is probably due to the catalysis of the metal oxide components in the S-UFA particles. After the S-UFA loading fraction greater than 30 wt %, the stability of the blends increases with the increment S-UFA content. This could be ascribed to the barrier effect of the S-UFA particles against the volatile pyrolyzed products.

ACKNOWLEDGMENTS

The authors would like to express their thanks to Guizhou Mingchuan Fly Ash Co., Ltd for providing ultrafine fly ash.

REFERENCES

1. Qu, P.; Zhou, Y.; Zhang, X.; Yao, S.; Zhang, L. J. *Appl. Polym. Sci.* **2012**, *125*, 3084.
2. Lunt, J. *Polym. Degrad. Stabil.* **1998**, *59*, 145.
3. Carrasco, F.; Pagès, P. *Polym. Degrad. Stabil.* **2008**, *93*, 1000.
4. Ray, S. S.; Yamada, K.; Ogami, A.; Okamoto, M.; Ueda, K. *Macromol. Rapid. Commun.* **2002**, *23*, 943.
5. Dorgan, J.; Lehermeier, J.; Palade, L.; Cicero, J. *Macromol. Symp.* **2001**, *175*, 55.
6. Jscobsen, S.; Degee, P. H.; Fritz, H. G.; Dubois, P. H.; Jerome, R. *Polym. Eng. Sci.* **1999**, *39*, 1311.
7. Rasal, R. M.; Janorkar, A. V.; Hirt, D. E. *Prog. Polym. Sci.* **2010**, *35*, 338.
8. Di Lorenzo, M. L. *Eur. Polym. J.* **2005**, *41*, 569.
9. Wu, T. M.; Chiang, M. F. *Polym. Eng. Sci.* **2005**, *45*, 1615.
10. Chieng, B. W.; Ibrahim, N. A.; Yunus, W.; Hussein, M. Z. *J. Appl. Polym. Sci.* **2013**, *130*, 4576.
11. Pivsa-Art, W.; Fujii, K.; Nomura, K.; Aso, Y.; Ohara, H.; Yamane, H. *J. Appl. Polym. Sci.* **2016**, *138*, DOI: 10.1002/app. 41856.
12. Penning, J. P.; Dijstra, H.; Pennings, A. J. *Polymer* **1993**, *34*, 942.
13. Vainiopää, S.; Rokkanen, P.; Törmälä, P. *Prog. Polym. Sci.* **1989**, *14*, 679.
14. Tachibana, Y.; Maeda, T.; Ito, O.; Maeda, Y.; Kunioka, M. *Polym. Degrad. Stabil.* **2010**, *95*, 1321.
15. Miao, P.; Wu, D.; Xu, G.; Zhao, C.; Yang, G. *Polym. Degrad. Stab.* **2010**, *95*, 1665.
16. He, F.; Li, S.; Vert, M.; Zhuo, R. *Polymer* **2003**, *44*, 5145.
17. Gutierrez-Villarreal, M. H.; Ulloa-Hinojosa, M. G.; Gaona-Lozano, G. J. *J. Appl. Polym. Sci.* **2008**, *110*, 163.
18. Wasantha, L. M.; Gunaratne, K.; Shanks, R. A. *Polym. Eng. Sci.* **2008**, *48*, 1683.
19. Chun, K. S.; Husseinsyah, S.; Osman, H. *Polym. Eng. Sci.* **2013**, *53*, 1109.
20. Wang, Y.; Mano, J. F. *Eur. Polym. J.* **2005**, *41*, 2335.
21. Furuhashi, Y.; Kimura, Y.; Yoshie, N.; Yamane, H. *Polymer* **2006**, *47*, 5965.

22. Raghavendra, S. C.; Khasim, S.; Revanasiddappa, M.; Prasad, M. A.; Kulkarni, A. B. *Mater. Sci.* **2003**, *26*, 733.
23. Potgieter-Vermaak, S. S.; Potgieter, J. H.; Kruger, R. A.; Spolnik, Z.; van Grieken, R. *Fuel* **2005**, *84*, 2295.
24. Kolstad, J. J. *J. Appl. Polym. Sci.* **1996**, *62*, 1079.
25. Taghvaei, A. H.; Shokrollahi, H.; Ebrahimi, A.; Janghorban, K. *Mater. Chem. Phys.* **2009**, *116*, 247.
26. Deepthi, M. V.; Sharma, M.; Sailaja, R. R. N.; Anatha, P.; Sampathkumaran, P.; Seetharamu, S. *Mater. Des.* **2010**, *31*, 2051.
27. Pan, P.; Liang, Z.; Cao, A.; Inoue, Y. *ACS Appl. Mater. Int.* **2009**, *1*, 402.
28. Lin, C. F.; Hsi, H. C. *Environ. Sci. Technol.* **1995**, *29*, 1109.
29. Miyata, T.; Masuko, T. *Polymer* **1997**, *38*, 4003.
30. Yasuniwa, M.; Iura, K.; Dan, Y. *Polymer* **2007**, *48*, 5398.